

First-principles study of the multi-mode anti-ferroelectric transition of PbZrO_3

Jorge Íñiguez,¹ Massimiliano Stengel,^{2,1} Sergey Prosandeev,³ and L. Bellaiche³

¹*Institut de Ciència de Materials de Barcelona (ICMAB-CSIC), Campus UAB, 08193 Bellaterra, Spain*

²*ICREA-Institució Catalana de Recerca i Estudis Avançats, 08010 Barcelona, Spain*

³*Physics Department and Institute for Nanoscience and Engineering, University of Arkansas, Fayetteville, Arkansas 72701, USA*

We have studied *ab initio* the phase transition in PbZrO_3 , a perovskite oxide usually presented as the prototypic anti-ferroelectric material. Our work reveals the crucial role that anti-ferrodistortive modes – involving concerted rotations of the oxygen octahedra in the structure – play in the transformation, as they *select* the observed anti-ferroelectric phase, among competing structural variants, via a cooperative trilinear coupling.

PACS numbers: 77.80.-e, 77.84.-s, 63.20.dk, 71.15.Mb

From a structural point of view, most ABO_3 perovskite oxides present phases that can be regarded as distorted versions of the cubic prototype [1–3]. Many are characterized by concerted rotations of the O_6 octahedra that constitute the basic building block of the lattice (e.g., SrTiO_3 , most manganites and nickelates). A second group presents off-centering displacements of the A and B cations, which typically result in a switchable ferroelectric (FE) polarization (e.g., BaTiO_3 or PbTiO_3). Finally, these two features appear combined in some cases (e.g., BiFeO_3 or LiNbO_3). Exceptions to these typical situations are uncommon, but are attracting growing interest. In particular, materials displaying an anti-polar cation displacement pattern, i.e. the so-called *anti-ferroelectric* (AFE) order, are currently a focus of attention for both fundamental and applied reasons [4–6].

Many phases characterized by rotations of the O_6 octahedra (anti-ferrodistortive or AFD modes henceforth) also display anti-polar displacements of the A cations. Such anti-polar distortions are typically a consequence of the AFD modes [7] and would not exist in their absence; the ensuing AFE order can thus be regarded as *improper* in nature. In contrast, here we are interested in materials usually described as *proper* AFEs, in which a phase transition accompanied by a dielectric anomaly is supposedly driven by a primary anti-polar order parameter. (We adopt the most common definition of a proper AFE transition [4].) PbZrO_3 (PZO) displays such a striking behavior, and is usually presented as the prototypic AFE crystal [8–11]. However, the nature of PZO's transition is far from being settled, as new experimental results and conflicting physical pictures have recently been reported [12, 13]. Hence, there is a need to clarify PZO's behavior and status as a model AFE. Here we present a first-principles investigation to that end.

Main modes and their couplings.– We followed the usual first-principles approach to the investigation of a non-reconstructive phase transition, taking advantage of the experimental knowledge of the high-temperature (cubic $Pm\bar{3}m$, with the elemental 5-atom unit cell) and low-temperature (orthorhombic $Pbam$, with a 40-atom unit

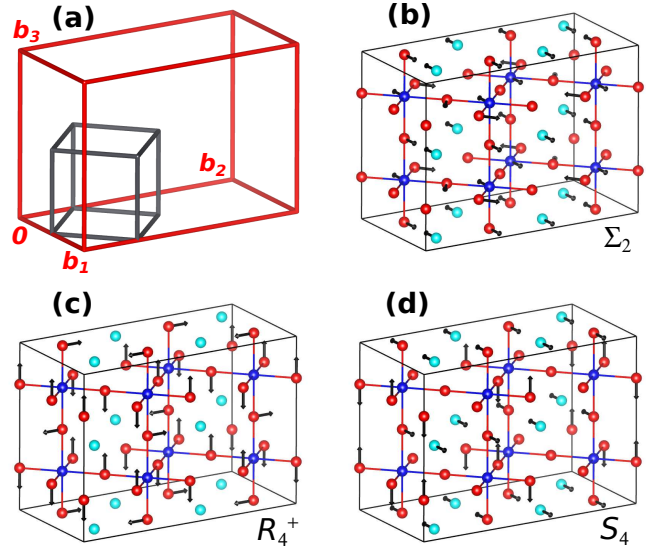


FIG. 1. (Color online) (a): Sketch of the 5-atom primitive cubic cell (small cube) and the $\sqrt{2} \times \sqrt{2} \times 2$ cell corresponding to PZO's AFE phase (large polyhedron). For the latter, the \mathbf{b}_i lattice vectors are shown (see text). (b), (c), and (d): Three main distortion modes that lead to PZO's ground state (see text). Symmetry labels indicated. Bonds between Zr (dark blue) and O (red) atoms are drawn. Note the characteristic AFE displacement of the Pb (cyan) atoms associated with the Σ_2 distortion.

cell) structures [14, 15]. The unit cell of the AFE $Pbam$ phase can be viewed as a $\sqrt{2} \times \sqrt{2} \times 2$ multiple of the elemental unit, as sketched in Fig. 1(a). More precisely, if $\mathbf{a}_1 = a(1, 0, 0)$, $\mathbf{a}_2 = a(0, 1, 0)$, and $\mathbf{a}_3 = a(0, 0, 1)$ define the ideal 5-atom cell in a Cartesian reference, the $Pbam$ cell vectors are given by $\mathbf{b}_1 = \mathbf{a}_1 - \mathbf{a}_2$, $\mathbf{b}_2 = 2(\mathbf{a}_1 + \mathbf{a}_2)$, and $\mathbf{b}_3 = 2\mathbf{a}_3$. As shown in Fig. 1(b), PZO's AFE distortion involves displacements of the Pb cations along the pseudo-cubic $[1\bar{1}0]$ direction, modulated according to the wave vector $\mathbf{q} = \mathbf{q}_\Sigma = 2\pi(1/4, 1/4, 0)/a$ of the first Brillouin Zone (BZ) of the 5-atom cell. (We give all vectors in the pseudo-cubic setting.)

We used standard methods based on density func-

tional theory (details in [16]) to relax the $Pm\bar{3}m$ and $Pbam$ phases, and got results [16] in good agreement with experiments [14, 15] and previous theoretical works [17, 18]. Then, we employed standard crystallographic tools [19] to identify the symmetry-adapted distortions connecting these two structures, and found three dominating ones [20]: (1) A Σ_2 component associated with the \mathbf{q}_Σ wave vector and which captures 36.0 % of the total distortion. This is the AFE_Σ displacement pattern sketched in Fig. 1(b). Interestingly, this distortion also has certain AFD character, as oxygen displacements reminiscent of an in-phase rotation about the \mathbf{b}_3 axis are clearly appreciated. (2) A R_4^+ component associated to $\mathbf{q}_R = 2\pi(1/2, 1/2, 1/2)/a$ and involving anti-phase rotations of the O_6 octahedra about the $[\bar{1}\bar{1}0]$ axis; see sketch in Fig. 1(c). This AFD distortion amounts to 59.7 % of the total. (3) A S_4 distortion associated to $\mathbf{q}_S = 2\pi(1/4, 1/4, 1/2)/a$ that captures 4.1 % of the total and is sketched in Fig. 1(d). This distortion too has a mixed character, combining AFE features with others that are reminiscent of AFD modes.

We then considered the simplest model that captures how the energy of PZO changes as a function of these three distortions of the cubic phase. Let Q_Σ , Q_R , and Q_S denote the respective amplitudes, which we normalize so that $Q_\Sigma = Q_R = Q_S = 1$ describe the situation at the $Pbam$ ground state. To fourth order, the energy has the form [19]:

$$\begin{aligned}
E = E_{\text{cubic}} + & \\
& A_\Sigma Q_\Sigma^2 + B_\Sigma Q_\Sigma^4 + A_R Q_R^2 + B_R Q_R^4 + \\
& A_S Q_S^2 + B_S Q_S^4 + C_{\Sigma RS} Q_\Sigma Q_R Q_S + \\
& D_{\Sigma R} Q_\Sigma^2 Q_R^2 + D_{\Sigma S} Q_\Sigma^2 Q_S^2 + D_{RS} Q_R^2 Q_S^2.
\end{aligned} \tag{1}$$

Interestingly, we find a trilinear coupling $C_{\Sigma RS}$ involving all three modes under consideration. Such a coupling, whose existence had been noticed already [13, 21], is cooperative in nature and provides a mechanism for the simultaneous occurrence of the involved distortions. In order to get a quantitative estimate of the model parameters, we investigated various paths to transit between the $Q_\Sigma = Q_R = Q_S = 0$ and $Q_\Sigma = Q_R = Q_S = 1$ states. Figure 2 shows the results; the quality of the fit to Eq. (1) (parameters in caption) is excellent [22].

Several conclusions can be drawn from these results. First, all three Σ_2 , R_4^+ , and S_2 modes are instabilities of the cubic phase when considered individually. The AFD instability is the dominant and strongest one, closely followed by the AFE mode; in contrast, the energy gain associated with the S_4 mode is clearly smaller. Next, note that all the biquadratic couplings in Eq. (1) are *competitive* in nature, i.e., we have $D_{\Sigma R}, D_{\Sigma S}, D_{RS} > 0$. Interestingly, the AFE and AFD instabilities are strong enough to coexist in spite of their mutual repulsion; in contrast, condensation of either the AFE or AFD distortion results in the stabilization of the S_4 mode. Finally,

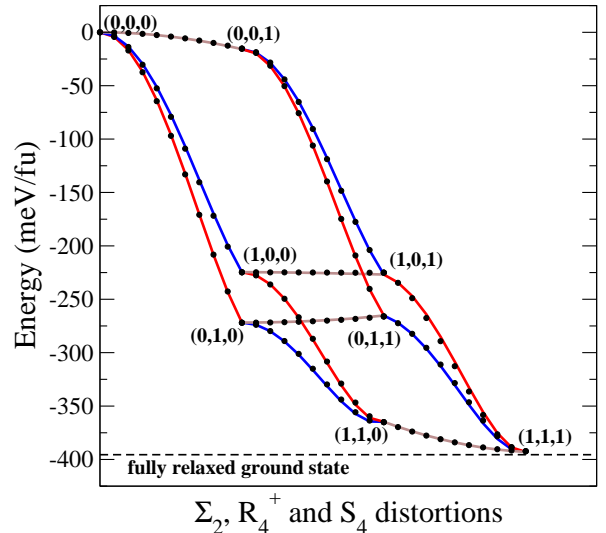


FIG. 2. (Color online) Circles: Computed energies of various structures defined by (Q_Σ, Q_R, Q_S) triads (see text; the triads for the limit and intermediate structures are indicated). Lines: Fit to Eq. (1); fitted parameters (meV per formula unit): $A_\Sigma = -337.3$, $B_\Sigma = 112.7$, $A_R = -420.9$, $B_R = 149.1$, $A_S = -16.4$, $B_S = 0.6$, $C_{\Sigma RS} = -48.4$, $D_{\Sigma R} = 131.7$, $D_{\Sigma S} = 22.4$, and $D_{RS} = 13.6$. For all triads we considered the equilibrium cell of the $Pbam$ phase in the calculations (note that the Q 's do not involve any strain); results using the relaxed cubic cell are very similar [16]. The dashed horizontal line marks the energy of the fully relaxed ground state.

and remarkably, the trilinear term has a considerable impact in the ground state energy: when going from $(1, 1, 0)$ to $(1, 1, 1)$ via relaxation of the S_4 distortion, the energy undergoes a considerable reduction, by about 27 meV per formula unit (fu). These three distortions together produce an energy gain of 392 meV/fu compared to the cubic phase. Full relaxation (via other structural modes not considered here) lead to a further energy decrease of only 3 meV/fu, which confirms the dominant character of Q_Σ , Q_R and Q_S .

Competing phases.— Earlier studies suggest that the equilibrium $Pbam$ phase of PZO competes with other FE, AFE, and AFD structures [17, 21, 23–25]. We thus ran a series of computer experiments to shed some light on why PZO chooses such an unusual phase over more common alternatives.

We computed the energy of several hypothetical PZO phases displaying combinations of the most typical AFD and FE displacement patterns. We also considered a number of AFE patterns similar to AFE_Σ but with different periodicities. To obtain the AFE_q states, we first displaced the Pb cations by hand along the $[\bar{1}\bar{1}0]$ direction with the spatial modulation of the targeted wave vector, and then let the structure fully relax while preserving the initial symmetry. (In some cases the relaxed structures present more complex Pb displacements than initially expected.) From the results, which are summarized in Ta-

TABLE I. Computed energies of PZO adopting several structures characterized by the presence of AFD (labeled using Glazer's notation [1]) and polar distortions. For the polar distortions, we indicate whether they are FE or AFE and the (approximate in some cases) direction along which the dipoles lie. In cases in which there is more than one AFE component, we only indicate the dominant wave vector. The structures with asterisk have the same space group as the ground state (gs), but their corresponding cells are different.

structure	$E - E_{\text{gs}}$ (meV/fu)	AFD dist.	polar dist.
$Pbam$ (gs)	0	$a^- a^- c^0$	AFE $[\bar{1}\bar{1}0]$ $\mathbf{q} = 2\pi(1/4, 1/4, 0)/a$
$Pm\bar{3}m$	375	-	-
$I4/mcm$	113	$a^- b^0 b^0$	-
$Imcm$	52	$a^- a^- c^0$	AFE $[\bar{1}\bar{1}0]$ $\mathbf{q} = 2\pi(1/2, 1/2, 1/2)/a$
$R\bar{3}c$	75	$a^- a^- a^-$	-
$Pnma$	35	$a^- a^- c^+$	AFE $\sim [110]$ $\mathbf{q} = 2\pi(0, 0, 1/2)/a$
$P4mm$	124	-	FE $[100]$
$Amm2$	91	-	FE $[110]$
$R3m$	58	-	FE $[111]$
$Ima2$	19	$a^- a^- c^0$	FE $[110]$
$R3c$	7	$a^- a^- a^-$	FE $[111]$
$Pbmm$	217	-	AFE $[\bar{1}\bar{1}0]$ $\mathbf{q} = 2\pi(1/2, 1/2, 0)/a$
$Pbam^*$	68	-	AFE $\sim [100]$ $\mathbf{q} = 2\pi(1/4, 1/4, 0)/a$
$Pbam^*$	60	-	AFE $\sim [100]$ $\mathbf{q} = 2\pi(1/8, 1/8, 0)/a$

ble I, a number of conclusions emerge. On one hand, the pure FE state $R3m$ is more stable than the purely AFD or AFE ones, although they all lie relatively far from the ground state (e.g., the $R3m$ solution lies at 58 meV/fu above). Combinations of FE and AFD distortions, on the other hand, can produce structures that are remarkably close to the ground state (the $R3c$ and $Ima2$ solutions lie at 7 meV/fu and 19 meV/fu, respectively). In fact, the energy difference between the $Pbam$ and $R3c$ or $Ima2$ phases is smaller than the energy associated with the trilinear term discussed above (27 meV/fu), which suggests that such a coupling is essential for the stabilization of the ground state. The central role played by the mutual interaction between modes is also corroborated by our results for the AFE $_{\mathbf{q}}$ phases: \mathbf{q}_{Σ} is not the most favorable modulation, suggesting that, in absence of the R_4^+ and S_4 modes, there would be no reason for the crystal to favor it over, e.g., $\mathbf{q} = 2\pi(1/8, 1/8, 0)/a$.

Phonon mode analysis.— The results discussed so far point to a crucial role played by the AFD distortions in stabilizing the observed antiferroelectric phase of PZO. It is therefore reasonable to speculate that condensation of the AFD modes may have an important impact on

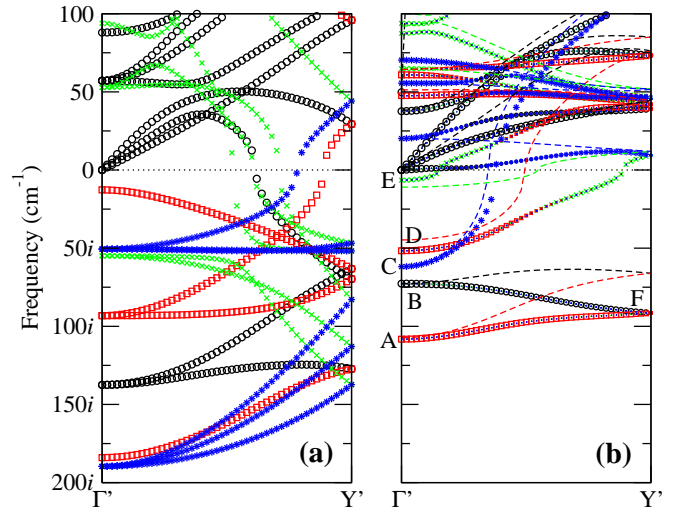


FIG. 3. (Color online) Phonon bands calculated along the Γ' - Y' line in the BZ of the 20-atom ($\sqrt{2} \times \sqrt{2} \times 2$) cell used to simulate the Q_R -distorted structure (see text). Primed labels denote wave vectors of this BZ. As a consequence of the folding, such a path encompasses four inequivalent segments in the BZ of the primitive cubic cell, each of which has been assigned a different color and symbol type: Γ - Σ (black circles), M - $\bar{\Sigma}$ (red squares), Z - S (green crosses), and R - \bar{S} (blue stars), where $\mathbf{q}_{\bar{S}} = -\mathbf{q}_{\Sigma}$ and $\mathbf{q}_{\bar{S}} = -\mathbf{q}_S$. The size of each symbol corresponds to the decomposition (projection) of a given mode into the four components described above. (a): Cubic phase ($Q_R = 0$). (b): Distorted phase ($Q_R = 1.13$). The dashed lines in (b) indicate the hypothetical phonon spectrum obtained by suppressing the interaction (off-diagonal terms) between \mathbf{q} -point pairs (see text). Only the low-energy part of the spectrum, including the unstable branches, is shown.

the unstable phonon branch associated with the polar (FE/AFE) modes. To verify this hypothesis, we calculated the phonon spectrum of PZO in two different configurations: first in the optimized cubic phase, and second in a phase where we optimized (by freezing it in by hand with an amplitude corresponding to $Q_R=1.13$) the relevant AFD ($a^- a^- c^0$) component, while keeping the other structural parameters identical to those of the cubic geometry.

The resulting phonon bands, calculated on a Γ' - Y' path in reciprocal space, are shown in Fig. 3. At $Q_R = 0$ [Fig. 3(a)] we recover the spectrum of the cubic reference, appropriately folded onto the smaller BZ of the $\sqrt{2} \times \sqrt{2} \times 2$ cell that we used to accommodate the AFD tilts. As previous authors noted [26], this phase presents multiple strong instabilities of both polar and AFD character, with the latter (particularly those at \mathbf{q}_R) appearing to dominate over the former. As expected, we observe a whole band of unstable polar distortions, which includes the FE and AFE patterns associated with most of the phases of Table I. Within this band, the FE mode at Γ' clearly dominates over the AFE modes.

The onset of the AFD distortions has a dramatic in-

fluence on the unstable region of the phonon spectrum [Figure 3(b)]. Most of the formerly unstable modes have been stabilized – only five branches with imaginary frequency persist. At the Γ' point of the folded BZ these are (from most to least unstable): (A) a c^+ -type AFD mode that would lead to the $Pnma$ structure of Table I; (B) a FE mode with the polarization oriented along $[1\bar{1}0]$ that would lead to the $Ima2$ phase; (C) a c^- -type AFD mode leading to $R\bar{3}c$; (D) an AFE mode with $\mathbf{q} = 2\pi(1/2, 1/2, 0)/a$ and polar distortions aligned with $[1\bar{1}0]$; (E) a similar AFE mode but with $\mathbf{q} = 2/\pi(0, 0, 1/2)/a$ that is also present in the $Pnma$ phase. All of these branches, except two, eventually become stable when moving away from Γ' . The surviving doublet (F) is predominantly of AFE_Σ character (80%) with a smaller S_4 component (20%). This is, of course, the distortion that directly leads to the ground-state structure. Remarkably, the doublet is now *more unstable* than the FE mode at Γ' [only AFD- c^+ appears to be stronger in panel (b)], confirming the crucial role played by Q_R in *selecting* a specific AFE ground state [27].

To understand which couplings are primarily responsible for such an outcome, we performed a further computational experiment. Note that, to leading order, the effect of a certain $Q_R = \bar{Q}_R$ distortion on the phonon spectrum is given by two types of terms: trilinear ones of the form $Q_{\mathbf{q}_1, s} Q_{\mathbf{q}_2, s'} \bar{Q}_R$, where s and s' label atomic displacements and $\mathbf{q}_1 + \mathbf{q}_2 + \mathbf{q}_R$ is a reciprocal lattice vector; biquadratic ones of the form $Q_{\mathbf{q}, s} Q_{\mathbf{q}, s'}^* \bar{Q}_R^2$. Hence, we recalculated the phonon bands of the \bar{Q}_R -distorted structure while suppressing the off-diagonal elements of the dynamical matrix that couple $(\mathbf{q}_1, \mathbf{q}_2)$ pairs. The result, shown as dashed lines in Fig. 3(b), clearly shows that the trilinear terms play a crucial role in pushing the zone-boundary doublet (F) to lower energies than the FE mode at Γ' , and effectively favors the occurrence of the former in the ground state.

Nature of PZO's phase transition.– PZO's AFE structure involves distortions of various symmetries, and it seems experimentally proved that all of them appear spontaneously at a single, strongly-discontinuous transformation upon cooling from the cubic phase [4, 11]. Our simulations do not incorporate thermal effects, which prevents us from discussing PZO's transition in a conclusive way. Yet, they provide some hints that are useful in light of recent experimental measurements in which simultaneous softening of multiple phonon modes was observed [12, 13]. Based on the fact that the acoustic branch was also involved in the softening, theoretical models have been formulated where the phase transition is rationalized in terms of flexoelectric couplings [12]. Note that in this recent model the ferroelectric branch is believed to drive the transition and, in line with earlier works [10], the AFD distortions are assumed to play a secondary role.

Let us begin by noting that, in principle, a strongly first-order transition like PZO's may or may not be accompanied by a significant mode softening. Our results are compatible with such a *quasi-reconstructive* transformation, of the sort that occurs in perovskite oxides sharing some of PZO peculiar features. A notable example is BiFeO_3 [28–31], which also presents stable phases lying far below the cubic phase, strong FE, AFE, and AFD instabilities, low-lying $R\bar{3}c$ and $Pnma$ polymorphs, etc.

Notwithstanding these considerations, a particular soft mode might still drive the transformation. Let us assume that the AFD R_4^+ mode plays such a role. (Our argument remains valid if we swap the roles of the R_4^+ and Σ_2 modes.) Then, let us consider the harmonic part of a Landau potential for the Σ_2 and S_4 modes, at the AFD transition temperature (T_R) at which a R_4^+ distortion of amplitude \bar{Q}_R materializes. We would have:

$$F(Q_\Sigma, Q_S) \sim [\tilde{A}_\Sigma (T_R - T_\Sigma) + \tilde{D}_{\Sigma R} \bar{Q}_R^2] Q_\Sigma^2 + [\tilde{A}_S (T_R - T_S) + \tilde{D}_{RS} \bar{Q}_R^2] Q_S^2 + (\tilde{C}_{\Sigma RS} \bar{Q}_R) Q_\Sigma Q_S, \quad (2)$$

where T_Σ and T_S are the critical temperatures for the corresponding instabilities, and all the \tilde{A} and \tilde{D} parameters are positive. Our calculations show that the AFD and AFE_Σ instabilities are similarly strong; thus, we can tentatively assume $T_R \gtrsim T_\Sigma$. In such conditions, if $[\tilde{A}_\Sigma (T_R - T_\Sigma) + \tilde{D}_{\Sigma R} \bar{Q}_R^2]$ is comparable in magnitude to $\tilde{C}_{\Sigma RS} \bar{Q}_R$, then the above harmonic term might present a combined $\Sigma_2 + S_4$ instability. In other words, the occurrence of a discontinuous AFD transition could *spark* the Σ_2 and S_4 distortions, resulting in a single $Pm\bar{3}m \rightarrow Pbma$ transformation. (Alternatively, if the conditions for the $\Sigma_2 + S_4$ instability occurred at $T_{\Sigma S} \lesssim T_R$, an intermediate phase could be observed between $T_{\Sigma S}$ and T_R .)

Regardless of whether we should view PZO's transition as a quasi-reconstructive one or a soft-mode driven one, the central role of the AFD modes (to stabilize the $Pbam$ phase over other alternatives or provide the induction mechanism through a trilinear coupling, respectively) is clear from our results. This is in line with the hypotheses made in [13] and questions the validity of models that treat the AFD distortions as a secondary effect [12].

In summary, our work has led to key insights concerning PZO's AFE transition. Most importantly, our results suggest that the multi-mode character of the transformation is essential to its very occurrence. In particular, we have found that AFD modes associated to oxygen octahedra rotations play a key role in *selecting* the experimentally observed AFE structure, over competing structural variants, via a cooperative trilinear coupling. Consequently, it does not seem appropriate to think of a primary AFE order parameter driving PZO's transition; rather, our results suggest a peculiar improper-like nature of the AFE order. PZO thus appears as a very

complex material, which poses the provocative question of whether its intricate behavior can be taken as representative of anti-ferroelectricity in perovskite oxides.

Work supported by MINECO-Spain (Grants No. MAT2010-18113 and No. CSD2007-00041). We also acknowledge support from Generalitat de Catalunya (2014 SGR 301) (JÍ and MS) and ONR Grants No. N00014-11-1-0384 and No. N00014-12-1-1034 (SP and LB). We used the facilities provided by the CESGA supercomputing center. Some figures were prepared using VESTA [32].

-
- [1] A. M. Glazer, *Acta Crystallographica B* **28**, 3384 (1972).
 [2] A. M. Glazer, *Acta Crystallographica A* **31**, 756 (1975).
 [3] D. M. Giaquinta and H.-C. zur Loye, *Chemistry of Materials* **6**, 365 (1994).
 [4] K. M. Rabe, “Antiferroelectricity in oxides: A reexamination,” in *Functional Metal Oxides* (Wiley-VCH Verlag GmbH & Co. KGaA, 2013) pp. 221–244.
 [5] X. Hao, *Journal of Advanced Dielectrics* **3**, 1330001 (2013).
 [6] L. Zhu and Q. Wang, *Macromolecules* **45**, 2937 (2012).
 [7] L. Bellaiche and J. Íñiguez, *Physical Review B* **88**, 014104 (2013).
 [8] E. Sawaguchi, H. Maniwa, and S. Hoshino, *Physical Review* **83**, 1078 (1951).
 [9] G. Shirane, E. Sawaguchi, and Y. Takagi, *Physical Review* **84**, 476 (1951).
 [10] M. J. Haun, T. J. Harvin, M. T. Lanagan, Z. Q. Zhuang, S. J. Jang, and L. E. Cross, *Journal of Applied Physics* **65**, 3173 (1989).
 [11] H. Liu and B. Dkhil, *Zeitschrift für Kristallographie* **226**, 163 (2011).
 [12] A. K. Tagantsev, K. Vaideeswaran, S. B. Vakhrushev, A. V. Filimonov, A. Shaganov, D. Andronikova, A. I. Rudskoy, A. Q. R. Baron, H. Uchiyama, D. Chernyshov, A. Bosak, Z. Ujma, K. Roleder, A. Majchrowski, J. H. Ko, N. Setter, and R. G. Burkovsky, *Nature Communications* **4**, 2229 (2013).
 [13] J. Hlinka, T. Ostapchuk, E. Buixaderas, C. Kadlec, P. Kuzel, I. Gregora, J. Kroupa, M. Savinov, A. Klic, J. Drahokoupil, I. Etxebarria, and J. Dec, *Physical Review Letters* **112**, 197601 (2014).
 [14] S. Teslic and T. Egami, *Acta Crystallographica B* **54**, 750 (1998).
 [15] H. Fujishita, Y. Ishikawa, S. Tanaka, A. Ogawaguchi, and S. Katano, *Journal of the Physical Society of Japan* **72**, 1426 (2003).
 [16] See Supplemental Material, which includes Refs. [12, 15, 18, 26, 33–40], for a description of the simulation methods employed and complementary results and commentary.
 [17] D. J. Singh, *Physical Review B* **52**, 12559 (1995).
 [18] S. Piskunov, A. Gopeyenko, E. Kotomin, Y. Zhukovskii, and D. Ellis, *Computational Materials Science* **41**, 195 (2007).
 [19] “Isotropy software suite,” iso.byu.edu.
 [20] The symmetry labels correspond to the setting with the origin at the *B* site.
 [21] S. Prosandeev, C. Xu, R. Faye, W. Duan, H. Liu, B. Dkhil, P. E. Janolin, J. Íñiguez, and L. Bellaiche, *Physical Review B* **89**, 214111 (2014).
 [22] It may seem surprising that a 4th-order model can reproduce so well the energetics of a material that undergoes a first-order transition. However, this situation is typical among perovskite oxides; see for example [41].
 [23] G. Shirane, *Physical Review* **86**, 219 (1952).
 [24] R. Kagimura and D. J. Singh, *Physical Review B* **77**, 104113 (2008).
 [25] S. E. Reyes-Lillo and K. M. Rabe, *Physical Review B* **88**, 180102 (2013).
 [26] P. Ghosez, E. Cockayne, U. V. Waghmare, and K. M. Rabe, *Physical Review B* **60**, 836 (1999).
 [27] The preference for the *Pbam* ground state over the *Pnma* ($a^-a^-c^+$) phase is not obvious from Fig. 3(b). Hence, it seems to rely on further anharmonic couplings (intermode and involving strain) not reflected in the shown phonon bands. See [16] for further comments on this.
 [28] G. Catalan and J. F. Scott, *Advanced Materials* **21**, 2463 (2009).
 [29] O. Diéguez, O. E. González-Vázquez, J. C. Wojdeł, and J. Íñiguez, *Physical Review B* **83**, 094105 (2011).
 [30] S. Prosandeev, D. Wang, W. Ren, J. Íñiguez, and L. Bellaiche, *Advanced Functional Materials* **23**, 234 (2013).
 [31] C. Cazorla and J. Íñiguez, *Physical Review B* **88**, 214430 (2013).
 [32] K. Momma and F. Izumi, *Journal of Applied Crystallography* **41**, 653 (2008).
 [33] G. Kresse and J. Furthmüller, *Physical Review B* **54**, 11169 (1996).
 [34] G. Kresse and D. Joubert, *Physical Review B* **59**, 1758 (1999).
 [35] J. P. Perdew, A. Ruzsinszky, G. I. Csonka, O. A. Vydrov, G. E. Scuseria, L. A. Constantin, X. Zhou, and K. Burke, *Physical Review Letters* **100**, 136406 (2008).
 [36] P. E. Blöchl, *Physical Review B* **50**, 17953 (1994).
 [37] X. Gonze, B. Amadon, P. M. Anglade, J. M. Beuken, F. Bottin, P. Boulanger, F. Bruneval, D. Caliste, R. Caracas, M. Cote, *et al.*, *Computer Physics Communications* **180**, 25822615 (2009).
 [38] X. Gonze and C. Lee, *Physical Review B* **55**, 10355 (1997).
 [39] N. Troullier and J. L. Martins, *Physical Review B* **43**, 1993 (1991).
 [40] M. Fuchs and M. Scheffler, *Computer Physics Communications* **119**, 67 (1999).
 [41] J. Íñiguez, S. Ivantchev, J. M. Pérez-Mato, and A. García, *Physical Review B* **63**, 144103 (2001).